Polymer Testing 84 (2020) 106378

Contents lists available at ScienceDirect

Polymer Testing

journal homepage: http://www.elsevier.com/locate/polytest

Test Method

# Photothermal microscopy applied to the study of polymer composites

Facundo Zaldivar Escola [a,b,*]

[a] Departamento de Física, Facultad de Ingeniería, UBA, Av. Paseo Colón 850, C1063ACV, Buenos Aires, Argentina
[b] Consejo Nacional de Investigaciones Científicas y Técnicas (CONICET), Argentina

ARTICLE INFO

*Keywords:*
thermal diffusivity
Photothermal microscopy
polymer composites

ABSTRACT

It is proposed to transfer the capabilities of a high sensitivity photothermal technique, developed by the group and widely used in the study of thermal properties of ceramics, metals and glass, to the study of polymer composites. The technique uses a sensing beam for the measurement of the thermal response of the sample due to local effects induced by heating with a modulated pump laser. With a simple spatial sweep of the beams on the sample surface, information on a micrometric scale of the thermal diffusivity of the material, distribution of phases and pores is obtained. Post-process analysis allows calculating average values of relevant properties such as thermal diffusivity, degree of crystallinity and distribution of aggregates. These measurements are performed at low laser powers (of the order of micro watts) avoiding the damage of the studied samples and turning this technique into a powerful tool of non-destructive characterization.

## 1. Introduction

The applications of polymers have grown with the beginning of the new century. Today there are many uses in all types of areas, such as coatings, adhesives, engineering materials, packaging, clothing, solid supports for organic synthesis, biomedicine, prostheses and their emerging applications in additive manufacturing (3D printing).

This huge field of applications leads to the constant development of new materials with improved properties for each purpose, as is the case of polymers based micro or nanocomposites that in recent years have been used in many industrial fields. They allow an improvement of the properties of the pure polymer such as its rigidity or can add some properties that are almost non-existent in raw materials, such as gas permeability, fire resistance, electrical and thermal conductivity [1,2]. The latter is particularly interesting as it offers new possibilities for the replacement of metal parts in electrical systems [3] or in flame retardants [4,5]. In addition, automotive, aerospace and related industries are interested in thermally conductive nanocomposite polymers, among which we can highlight those based on conductive particles such as carbon nanotubes, graphene [6], metals [7], graphite [8] and expanded graphite [9–11].

The appearance of new materials presents the challenge of developing new versatile techniques for their characterization. In particular, the mechanical and thermodynamic properties require the development of specific techniques that discriminate the surface from the volume or even determine the gradient of properties generated by material treatments. This discrimination becomes particularly difficult when the substrate is of the same composition as the treated zone.

Although it is possible to identify the presence of the different metastable phases by means of X-ray diffraction techniques at grazing incidence, microstructural characterization is a problem that these techniques do not solve. X-ray diffraction provides information on the phases obtained but lacks of good spatial resolution, handling sample volumes above 1mm3. With microfocus systems, smaller volumes can be analyzed, but it is not suitable for sweeping thick samples (due to the penetration of X-rays). Electronic scanning microscopy (SEM) in conjunction with X-ray energy scattering spectroscopy (EDS) provides a mapping of the atomic composition for sample volumes of the order of 1–10μm3, but does not provide information on the degree of crystallization. Diffraction of backscattered electrons (EBSD) provides the complete information of the microstructure but at the expense of a high cost, a complex sample preparation and a high acquisition and processing time consumption. There are also difficulties in the measurements associated with characteristics of each technique that produce undesirable effects on the sample. A clear example of this can be seen in an SEM microscope where due to the intensity of the electron beam, irreversible damage can occur in the observed area of some polymers [12,13].

Previous works of the group showed that methods based on photothermal techniques can display a high contrast between the different

* Departamento de Física, Facultad de Ingeniería, UBA, Av. Paseo Colón 850, C1063ACV, Buenos Aires, Argentina.
*E-mail address:* fzaldivar@fi.uba.ar.

https://doi.org/10.1016/j.polymertesting.2020.106378
Received 6 August 2019; Accepted 23 January 2020
Available online 27 January 2020

phases due to their distinct thermal diffusivity. Mapping structures with micrometric resolution, the study of homogeneity, composition and phase transformations in a diverse set of materials such as ceramics, metals, glass and thin layers have been achieved [14–17].

The thermal response of a material is given by the value of its thermal diffusivity ($D$), which characterizes the heat conduction, its effusivity (e), which defines the thermal contact between two surfaces, and its conductivity (κ), which determines the heat flow associated with a given temperature gradient.

In materials of industrial use it is of great interest to be able to predict and understand their behavior. For example, in computational modeling of heat transfer under stationary or transitory conditions, an adequate knowledge of these physical parameters, such as the properties of each of the constituents at microscopic scales, is fundamental.

It should be noted that the nature of the molecular structure of polymers makes the properties of these materials strongly dependent on temperature. Although a series of correlations have been reported associating structural variables such as polymer molecular weight, crystallinity, orientation, etc. with thermal properties [18–20], the development of precise techniques for such measurements is still essential given that, due to factors such as resistance to thermal contact and inhomogeneities in the sample, these measurements in polymers have always presented difficulties.

Several techniques capable of polymers thermal properties characterization can be highlighted, the flash laser and the hot-wire technique being the most commonly used [21,22]. The first is used for the measurement of thermal diffusivity, heat capacity and thermal conductivity but lacks of good spatial resolution since the pulse absorbed on the sample surface to be measured diffuses through the entire thickness of the sample [23,24]. The second is used for the measurement of thermal conductivity with advantages over traditional calorimetry methods that cannot measure this parameter at room temperature, but the information obtained also comes from the full volume of the sample and cannot be used with electrically conductive samples [22,25,26].

Thus, there is currently no simple and unifying technique capable of revealing the microstructure of the polymer, giving simultaneous information of homogeneity (identifying, for example, crystallized zones and different species) with a simple sample preparation, without damage during the measurement and with short processing times.

In this work we propose the usage of the Photothermal Microscopy [27], to respond to such inquiries. It is based on the measurement of the thermal response of the sample due to local effects induced by heating with a modulated laser. The method consists of detecting the reinjected signal in an optical fiber from the reflection on the sample surface of a second probe laser. The usage of fiber optic technologies makes this system a robust tool, preserving the alignment of lasers perpetually. By performing maps of the photothermal signal, the distribution of the constituents can be found and histograms displaying the homogeneity of the sample can be performed.

The study carried out on samples of PMMA (Polymethylmethacrylate) and a polymeric composite of PP (Polypropylene) + 5% Quartz is presented. The studied samples are only examples to show the capabilities of this technique that can be extended to many types of polymers or polymer composites.

## 2. Experimental

In this section, the fundamental aspects of the proposed technique are described. Afterwards the samples studied and the measurement process are detailed.

### 2.1. The technique

The instrument used has been completely described in a previous work [17]. Fig. 1 shows a simplified schematic of the experimental configuration.

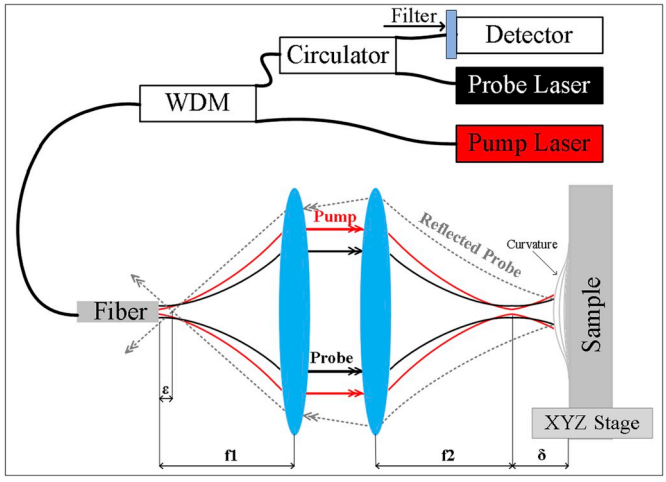


**Fig. 1.** Experimental configuration.

A fiber coupled laser that emits at 660 nm is used as a pump beam modulated in intensity to excite the sample and another one that emits at 785 nm is used as a CW probe beam to sense the thermal response of the material. The lasers are combined in a single mode fiber by means of a wavelength division multiplexer (WDM). Both beams emerge from the fiber passing through a lens system that directs and focuses them at a distance δ from the sample surface. A portion of the pump beam is absorbed by the surface and increases the local temperature of the sample. This increment in temperature produces an expansion modulated at the excitation frequency that curves the surface at the pump beam impinging location. The probe beam is reflected on the surface and returns through the lens system, focusing at a distance ε from the edge of the fiber. The reinjected portion reaches the detector passing through the WDM and a circulator. It should be noted that a filter is interposed before the detector to prevent that any reflection of the pump beam reaches it.

To ensure the absorption of the pump beam and reflection of the probe beam, a nanometric layer of platinum is deposited on the surface. The layer is thin enough (~50 nm) so that the lateral heat conduction, within the platinum layer, can be neglected [28].

The reinjection signal has a modulated component at the pump beam frequency (ω) due to the defocusing generated by the surface curvature that modifies the transmission through the fiber (curvature effect). In this way, the signal is amplified and filtered by a lock-in amplifier, obtaining the information of the amplitude and the phase delay (with respect to the pump beam) of the power of the reinjected beam.

This signal is modeled as Equation (1) [27]:

$$S_\omega = \frac{\lambda_z}{\kappa}\left(P_{probe} R \frac{\partial t_r}{\partial Q^{'}} \frac{\eta P_\omega z_0}{16\pi\sigma_{Pump}^2} C_{cal}\right) h(\omega/\omega_0) \quad (1)$$

where parameters $P_{probe}$, $R$, and $z_0$are associated with the probe beam, being its power, the reflectivity of the superficial layer at its wavelength and its confocal parameter, respectively. The parameters $P_\omega$, $\eta$ and $\sigma_{Pump}$ are associated with the pump beam, being its power modulation amplitude, the absorption of the surface layer at its wavelength, and its beam radius (½ the beam waist) on the surface, respectively. The parameter $t_r$ denotes the reinjected portion of the probe beam in the fiber and the term $\partial t_r/\partial Q^{'}$denotes the variation of said reinjection with the change of the inverse of the radius of curvature ($Q^{'}$) induced by the pump beam. The $C_{cal}$, is the detector calibration constant. The parameters $\kappa$ and $\lambda_z$correspond to the sample thermal conductivity and thermal expansion coefficient.

The magnitude $\omega_0$, called critical frequency $(2\pi f_0)$, is the frequency for which the heat diffuses a distance equal to the pump beam radius

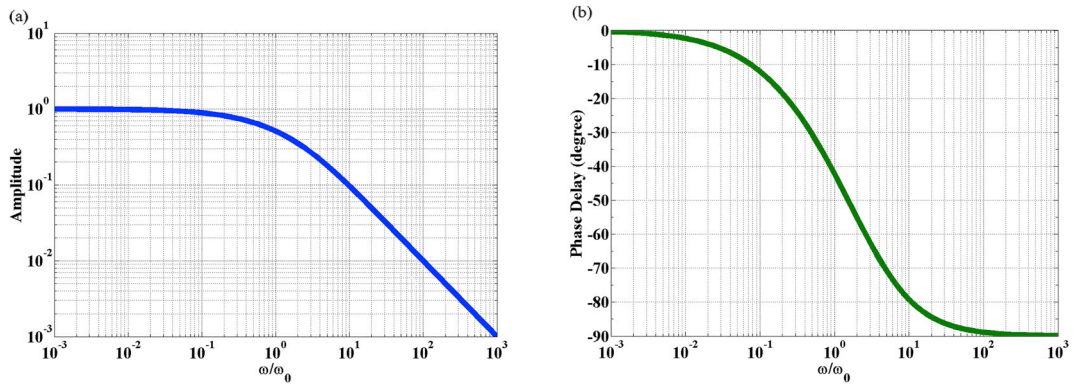


**Fig. 2.** Theoretical curves of the frequency response (adimensionalized by $\omega_0$) of the amplitude and phase delay of the curvature effect ($h$) [27].

($\sigma_{Pump}$) in a period of modulation. It only depends on pump beam radius and the thermal diffusivity ($D$) at the impinging location as described in Equation (2):

$$\omega_0 = \frac{2D}{\sigma^2_{Pump}} \tag{2}$$

The function $h$ is complex and is plotted against the frequency in Fig. 2, where it can be observed that, after overcoming the critical frequency $\omega_0$, the amplitude decays with slope $-1$ (in log-log scale) and at high frequencies a jump of $\pi/2$ in the phase delay of the signal with respect to the modulation can be noticed.

The measurement of the thermal diffusivity of the micrometric zone excited by the pump beam is obtained by fitting the experimental data (corresponding to the reinjection signal measured by the Lock-in amplifier when the modulation frequency of the pump beam is changed) by the theoretical curves of Fig. 2. In fact, this fit allows the determination of the critical frequency that is converted to diffusivity values by means of Equation (2).

It should be noted that the dimensionless photothermal signal amplitude and phase delay theoretical curves are universal and do not depend on the material or the experiment parameters. This leads to the fact that the phase delay at a fixed modulation frequency can be used to obtain the critical frequency (and therefore the thermal diffusivity) directly, which speeds up the measurements, allowing spatial sweeps with great speed and avoiding overheating the sample. This is achieved from the construction of a calibration curve that arises from the inversion of the phase delay graph axes [16,29].

From the slope of the curve to the critical frequency a sensitivity for the diffusivity measurement of 5.9%/degree is obtained.

On the other hand, the reinjected signal has a continuous component ($SDC$) proportional to the reflectivity of the surface at the probe beam wavelength.

The control of the sample position was carried out by means of a motorized unit XYZ that allows focusing and sweeping the surface in order to make maps of the photothermal signal and know its homogeneity.

### 2.2. Samples studied and procedure

In order to show the capabilities of the technique for the study of polymers and polymer composites, an exhaustive study of the photothermal signal as a function of the position was carried out in two types of samples with very different characteristics.

The first one, labeled as sample M1, consisted of a commercial sheet of PMMA (TEDPELLA code: 260226) with a nominal thickness of 1 mm. In a first stage, the photothermal signal measurement was performed as a function of the modulation frequency of the pumping beam in one pixel for 30 equidistant values in logarithmic scale between 257Hz and 50007Hz. This measurement (not shown) was used to estimate the critical frequency of the material and thus defines the frequency to be used in a spatial sweep. Then a 40 × 40 pixel spatial scan was performed (step 9.3 μm × 6.6 μm) measuring at a fixed modulation frequency, $f = 2467Hz$, with an integration time of the Lock-in of 100 ms and waiting 1s between measurements. The pump beam radius in this case was $\sigma = 2.9\mu m$.

The second sample studied, labeled as sample M2, consisted of a polymer composite manufactured by the Group of Mechanical Properties and Fracture, of the Institute of Polymers Technology and Nanotechnology (ITPN, Argentina). This composite consists of a commercial polypropylene (PP) matrix provided by Petroquímica Cuyo (Code: PP1102H) with 5 wt% of quartz particles used as reinforcement. The manufacturing process of this sample, that results in a sheet of 1 mm of nominal thickness and with a quartz particle sizes distribution ranging from submicron values to 8.5 μm, is described in Ref. [30]. Given the inhomogeneity of the sample and the strong dispersion of particle sizes, the study in this case requires a deeper analysis.

In a first stage, a study was carried out in a zone containing a single quartz particle. For this, 15 spatial sweeps of 23 × 31 pixels were performed (step ~ 1 μm), measuring each map at a different frequency, equidistant in logarithmic scale, between 1497Hz and 149797Hz, with an integration time of the Lock-in of 1s and waiting 10s between measurements.

In the second stage and, having determined the average critical frequency of the majority material (PP), a spatial sweep of 170 × 220 pixels was carried out (step ~ 1 μm), measuring at a fixed frequency $f = 14979Hz$with an integration time of the Lock-In of 100 ms and waiting 1s between measurements.

The pump beam radius in both those stages was $\sigma = 1.5\mu m$.

The powers of the pump (average) and probe beams used for all the measurements in the different samples were $P_{Pump} = 60.5\mu W$and $P_{probe} = 58.4\mu W$.

The DC component ($SDC$), the amplitude and the phase delay at the frequency of the pump beam of the signal reinjected into the fiber were acquired in each zone of a sample.

A simple analysis of equation (1) allows predicting the relative photothermal signal levels according to the pump beam impinging location. For either, spatial or frequency sweep, if the system parameters are maintained, the signal will be determined by the term "$\lambda_z/\kappa$" of each material. In the particular case study, the thermal conductivity and expansion coefficients of PP and quartz have been reported in different works [31–33] and it can be seen that areas of pure PP will have photothermal signal levels up to 3200 times higher than those of pure quartz. This considerable difference between the relative signals extends to a large number of polymers compared to samples widely studied by the proposed technique such as ceramics, glasses and metals. As a consequence, the power of the beams can be reduced thousands of times, maintaining usual signal levels (~100–1000 μV), without heating the sample. This strong reduction in power causes that the photothermal

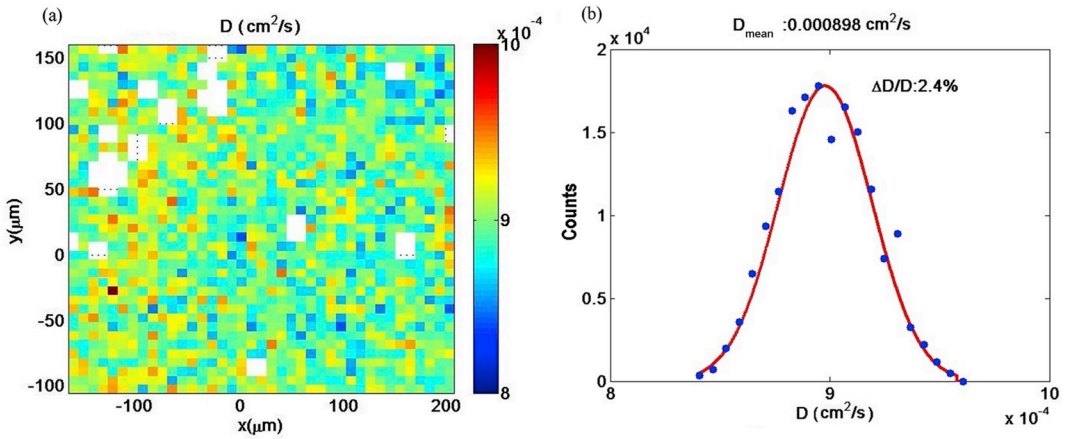


**Fig. 3.** Sample M1. (a) Thermal diffusivity map (40 × 40 pixels), the white areas correspond to values where the photothermal signal is canceled due to pores, scratches or dust particles. (b): Diffusivity histogram. The ΔD/D factor accounts for the precision of the technique. The fluctuations in the map are due to the noise of the measurements.

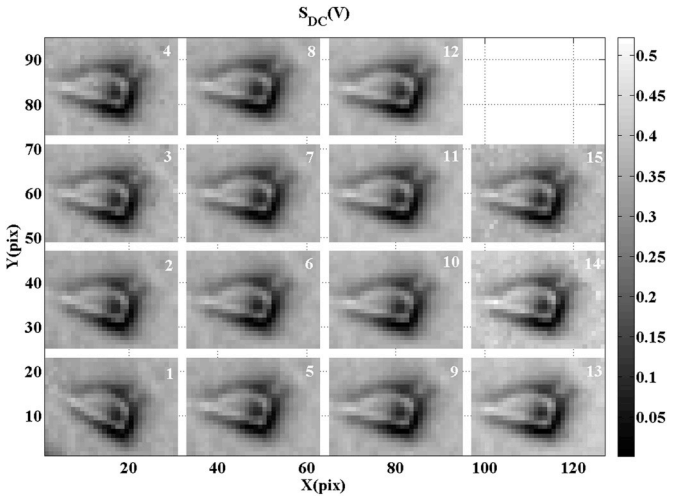


**Fig. 4.** Sample M2. Multimap of the DC component (*SDC*) of the reinjection signal. The number inside each map indicates the order of the sweep. Pixel size ~ 1 μm.

signal will fall below detection levels in areas of pure quartz. However, the reinjection signal *SDC* will be equivalent to those in the areas of PP since it depends mainly on the surface layer. This fact allows locating the zones with quartz clusters and differentiating them from the pores, since in these zones the photothermal signal and the *SDC* signal will be null.

## 3. Results

In Fig. 3(a) a thermal diffusivity map measured on sample M1 is observed in an area of approximately 350 μm × 250 μm. Fig. 3(b) shows the histogram of the diffusivity map. A mean diffusivity value of $D_{mean} = 0.000898 cm^2/s$consistent with the bulk values reported for this material at room temperature [34] can be observed.

Since a highly homogeneous sample has been measured, the factor $\Delta D/D = 2.4\%$accounts for the precision of the technique. On the other hand the accuracy (absolute position of the mean value, i.e. calibration) of the technique is dominated by the uncertainty in the determination of the beam size, being 15%.

Fig. 4 shows the different maps acquired over the same area for each frequency (Multimap) of the signal *SDC* for sample M2. The modulation frequency for each spatial sweep grows from bottom to top and from left to right. The presence of a cluster can be noted in each sweep whose repeatability in the position guarantees the stability of the sweep.

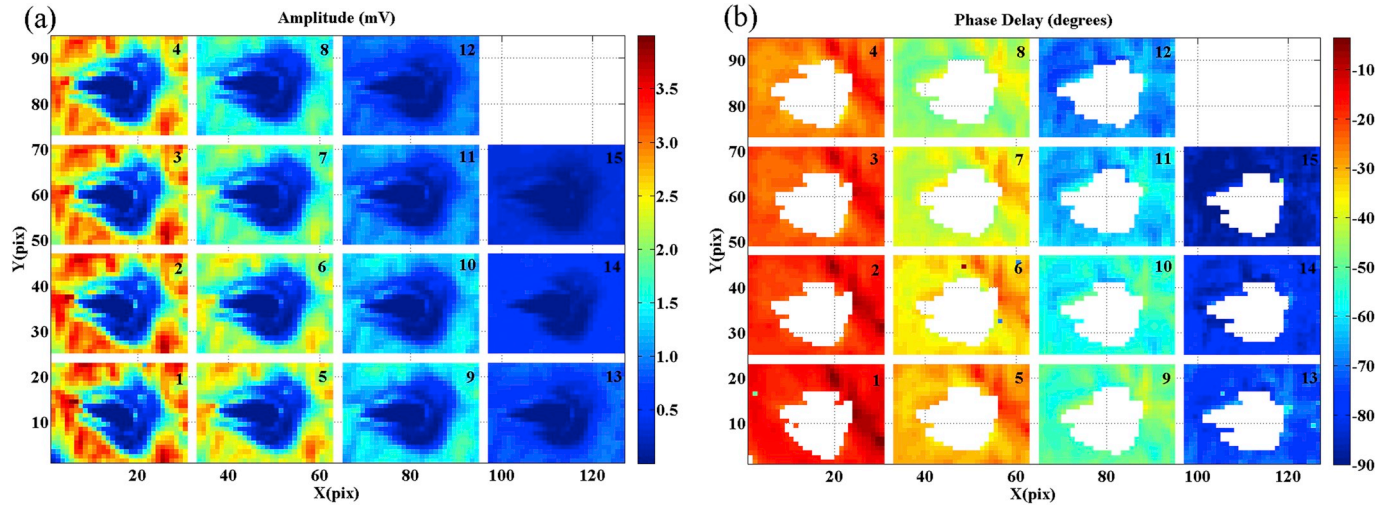


**Fig. 5.** Sample M2. Multimap of the measurements of (a) amplitude and (b) phase delay. White zones correspond to the areas where the amplitude signal falls below the noise level. The number inside each map indicates the order of the sweep. Pixel size ~ 1 μm.

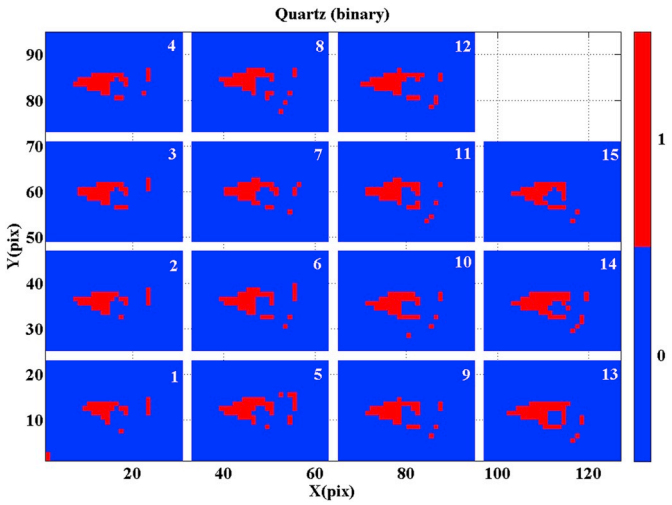


**Fig. 6.** Sample M2. Binary multimap corresponding to areas with pure quartz. The number inside each map indicates the order of the sweep. Pixel size ~ 1 μm.

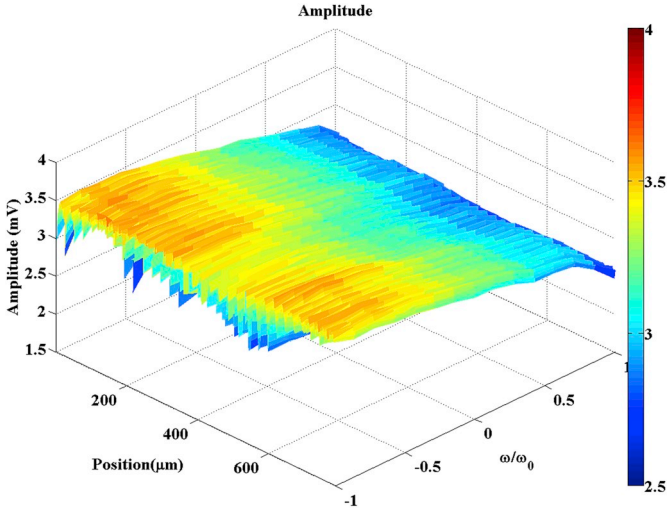


**Fig. 7.** Sample M2. Map of Amplitude vs. "position"-Frequency (normalized by the critical frequency estimated for the PP). Null signal zones (either by the presence of pores or quartz) have been removed. The expected trend corresponding to the curves of Fig. 2(a) can be observed.

The multimaps of the amplitude and phase delay measurements for the sample M2 are shown in Fig. 5(a) and Fig. 5(b), respectively.

By distinguishing the zones of null signal amplitude but not null *SDC* signal, the location of the quartz clusters can be recognized. This procedure is carried out starting from the construction of the amplitude and *SDC* signal binary matrices. The binarization of these matrices was done by choosing a cut-off threshold for each map that corresponds to the average value of the measured area minus two times its standard deviation. The "pixel by pixel" product of the binary *SDC* signal matrix, by the negated binary matrix of the amplitude signal, allows the zones with quartz to be revealed. The result of this process is shown in Fig. 6.

In order to show the correspondence between the pixel to pixel photothermal signal and the graphics of Fig. 2, the amplitude and phase delay maps were plotted, in the "position"-"modulation frequency" plane. The "position" in this case corresponds to the consecutive numbering of the pixels measured in a spatial sweep. For example, in a spatial scan of $23 \times 31$pixel for a given frequency, the "position" will go from 1 to 713 (pixels). Knowing the pixel size (~1 μm); we can

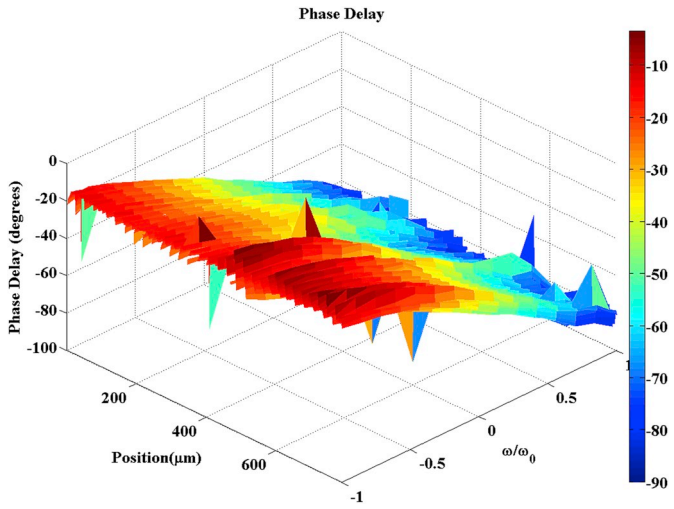


**Fig. 8.** Sample M2. Map of Phase Delay vs. "position"-Frequency (normalized by the critical frequency estimated for the PP). Null signal zones (either by the presence of pores or quartz) have been removed. The expected trend corresponding to the curves of Fig. 2(b) can be observed.

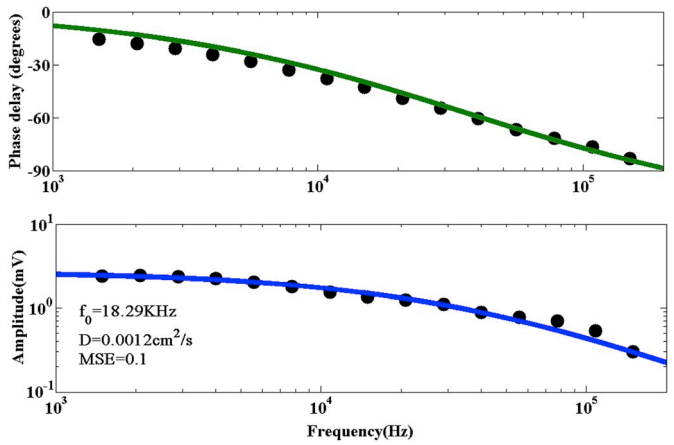


**Fig. 9.** Sample M2. Graphs of Amplitude and Phase delay averaged over the total swept area for each frequency and the adjustment by the theoretical curves of Fig. 2. It includes the values of critical frequency ($f_0$), average thermal diffusivity (D) and the mean squared error of the adjustment (MSE).

transform this scale into length units. Fig. 7 and Fig. 8 show these maps, where zones without photothermal signal (noise) have been removed and scale position has been changed to microns.

It should be noted that all the measurements are local and with micrometric resolution. To compare with the bulk mean values reported, an average pixel to pixel should be performed, that is, the average over the entire swept area at each frequency, and then to perform the adjustment by the theoretical curves of Fig. 2. Fig. 9 shows this adjustment from which an average thermal diffusivity of $D = 0.0012\text{cm}^2/\text{s}$ is obtained, which is consistent with the interval of values of thermal diffusivity $[0.0009 - 0.0012]\text{cm}^2/\text{s}$ that can be estimated from Equation (3):

$$D = \frac{\kappa}{\rho C_p} \tag{3}$$

for the reported values of heat capacity ($C_p = (1700 - 1900)10^{-6}/\text{K}$), thermal conductivity ($\kappa = (0.1 - 0.22)\text{W/mK}$), and density ($\rho = 0,91\text{g/cm}^3$) of bulk polypropylene [31].

The analysis presented shows the feasibility of using the proposed technique for the characterization of polymers and polymer composites.

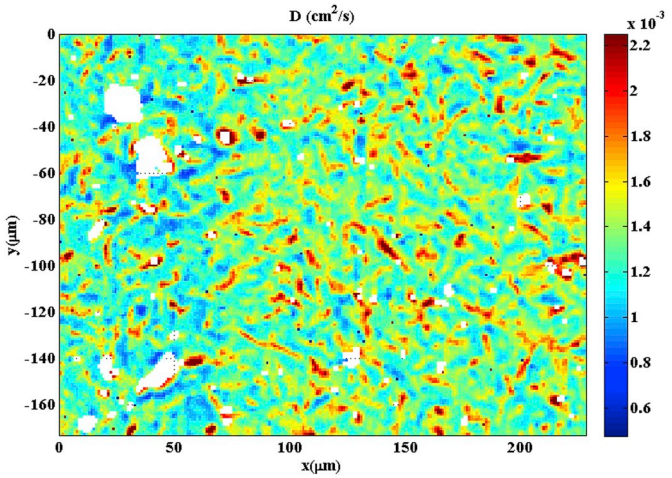


**Fig. 10.** Diffusivity map of the measured area. The area without a signal either by the presence of pores or quartz is plotted in white. It can be seen the distribution of crystalline phases (zones with vermicular shape of larger diffusivity) and amorphous (lower diffusivity background).

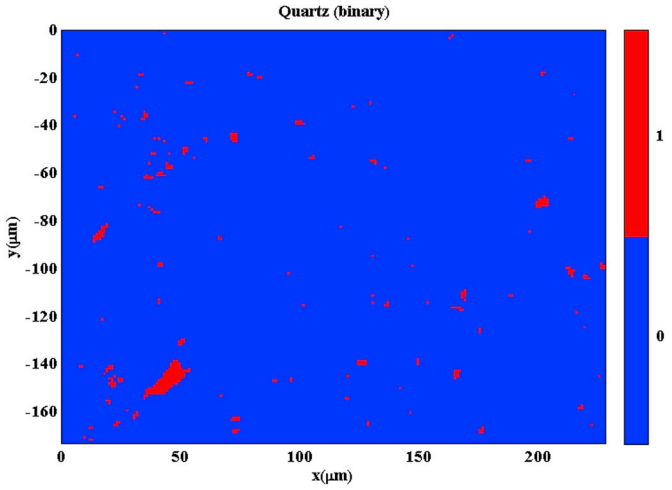


**Fig. 11.** Binary map of areas with pure quartz.

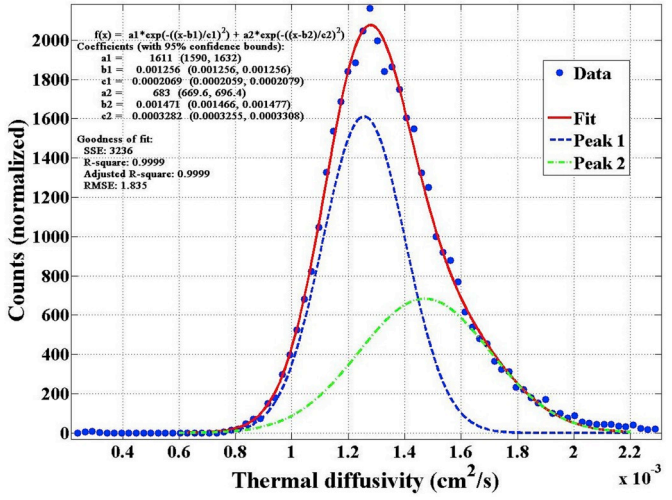


**Fig. 12.** Thermal diffusivity histogram of measured area shown in Fig. 10 and two Gaussian peaks adjustment for SOR estimation.

As an example of the capabilities of the technique, a map measured on the sample M2 in an area of 230 μmx130μm is presented in Fig. 10. The map of quartz clusters is shown in Fig. 11, where an inhomogeneous distribution of clusters can be observed.

Unlike PMMA (sample M1), which is completely amorphous, PP has a crystalline phase coexisting with an amorphous matrix. The map in Fig. 10 shows the existence of zones with vermicular shape of larger thermal diffusivity than the amorphous matrix, which can be assigned to the crystalline phase. These structures were not seen on the map shown for the PMMA, consistent with its amorphous nature (see Fig. 3).

A corroboration of what has been said arises from the comparison of the measurement of the degree of crystallinity of the sample M2 by means of the Differential Scanning Calorimetry technique (DSC) [35] with the structures occupation rate (*SOR*) over the swept area. The degree of crystallinity by DSC was measured by the Group of Mechanical Properties and Fracture of the ITPN (Argentina), where a value of (42 ± 2)% was obtained.

The *SOR*was estimated from the two Gaussian peaks adjustment of the histogram of map in Fig. 10, shown in Fig. 12. The area of each Gaussian peak has information on the occupation rate of each species. The peak centered on the highest value of thermal diffusivity was assigned to the crystalline phase and its area ($A_2$) was compared with the area occupied by the other peak ($A_1$). In this way, the *SOR*was estimated using Equation (4):

$$SOR = \frac{A_2}{(A_1 + A_2)} = (40.2 \pm 1.2)\% \quad (4)$$

where each area was calculated from the integrals of the Gaussians curves and the uncertainty from the errors propagation, considering the coincidence interval of the adjustment of Fig. 12 as the error in each parameter. It can be seen that within the error, the *SOR*obtained is in accordance with the value obtained by the DSC technique.

## 4. Conclusions

A powerful photothermal technique, for the local characterization of polymers and polymer composites has been presented. The technique allows, with a simple scan of 1s per pixel, the determination of thermal diffusivity with micrometric spatial resolution, a property that allows exposing with high contrast the different phases of a sample. The realization of photothermal signal maps allows characterizing the distribution of phases and pores.

Maps measured over the same area at different frequencies has allowed to show the great scan stability and the correspondence between the photothermal signal measured at each pixel with the theoretical curves of the photothermal model. The average values of thermal diffusivity on the swept areas for PMMA and PP are in agreement with the values reported for the same materials in bulk.

On the other hand, a map of thermal diffusivity has been shown on a highly homogeneous PMMA sample.

The histogram of this sweep provides a reference for the precision of the technique from the factor ΔD/D, being 2.4%. With this precision the presence of structures on areas with PP of the sample M2 can be revealed, assigned to the crystalline phase of said material. Through the analysis of the diffusivity histogram of the measured area the occupation rate of this phase, being (40.2 ± 1.2)% was determined, a value consistent with the degree of crystallinity measured by the DSC technique.

It should be noted that the study could be done with very low power (order of the micro watts), so the material is not affected by the study, proof of this are the multiple sweeps carried out on the same area where no degradation is observed.

## Acknowledgements

The author wishes to acknowledge the contributions of Celina R. Bernal from Group of Mechanical Properties and Fracture of the ITPN.

This work was supported by the grant [UBACyT # 20020170100137BA] from the University of Buenos Aires and the grant [PICT2015-1523] from the ANPCyT;

## Appendix A. Supplementary data

Supplementary data to this article can be found online at https://doi.org/10.1016/j.polymertesting.2020.106378.

## Data availability

The processed data required to reproduce these findings are available to download from [https://drive.google.com/drive/folders/10TspboQ4-tneTYN5yM_-9QsXppqCZDVq?usp=sharing].

## References

[1] B. Weidenfeller, M. Anhalt, S. Kirchberg, Thermal diffusivity and mechanical properties of polymer matrix composites, J. Appl. Phys. 112 (2012), 093513, https://doi.org/10.1063/1.4764098.
[2] M. Gresil, Z. Wang, Q. Poutrel, C. Soutis, Thermal diffusivity mapping of graphene based polymer nanocomposites, Sci. Rep. 7 (2017) 5536, https://doi.org/10.1038/s41598-017-05866-0.
[3] J. Kratochvíla, A. Boudenne, I. Krupa, Effect of filler size on thermophysical and electrical behavior of nanocomposites based on expanded graphite nanoparticles filled in low-density polyethylene matrix, Polym. Compos. 34 (2) (2013) 149–155, https://doi.org/10.1002/pc.22387.
[4] M. Murariu, A.L. Dechief, L. Bonnaud, Y. Paint, A. Gallos, G. Fontaine, P. Dubois, The production and properties of polylactide composites filled with expanded graphite, Polym. Degrad. Stabil. 95 (5) (2010) 889–900, https://doi.org/10.1016/j.polymdegradstab.2009.12.019.
[5] A. Laachachi, N. Burger, K. Apaydin, R. Sonnier, M. Ferriol, Is expanded graphite acting as flame retardant in epoxy resin, Polym. Degrad. Stabil. 117 (2015) 22–29, https://doi.org/10.1016/j.polymdegradstab.2015.03.016.
[6] M.M. Zhang, H.X. Yan, C. Gong, F.F. Zhang, Hyperbranched polysiloxane functionalization of graphene oxide for improved mechanical properties of cyanate ester nanocomposites, J. Compos. Mater. 49 (8) (2015) 939–948, https://doi.org/10.1177/0021998314527778.
[7] W. Zhou, S. Qi, Q. An, H. Zhao, N. Liu, Thermal conductivity of boron nitride reinforced polyethylene composites, Mater. Res. Bull. 42 (10) (2007) 1863–1873, https://doi.org/10.1016/j.materresbull.2006.11.047.
[8] G. Chen, D. Wu, W. Weng, C. Wu, Exfoliation of graphite flake and its nanocomposites, Carbon 41 (3) (2003) 619–621, https://doi.org/10.1016/S0008-6223(02)00409-8.
[9] W. Zheng, S.C. Wong, H.J. Sue, Transport behavior of PMMA/expanded graphite nanocomposites, Polymer 43 (25) (2002) 6767–6773, https://doi.org/10.1016/S0032-3861(02)00599-2.
[10] B. Debelak, K. Lafdi, Use of exfoliated graphite filler to enhance polymer physical properties, Carbon 45 (9) (2007) 1727–1734, https://doi.org/10.1016/j.carbon.2007.05.010.
[11] S. Ganguli, A.K. Roy, D.P. Anderson, Improved thermal conductivity for chemically functionalized exfoliated graphite/epoxy composites, Carbon 46 (5) (2008) 806–817, https://doi.org/10.1016/j.carbon.2008.02.008.
[12] D. T Grubb, Radiation damage and electron microscopy of organic polymers, J. Mater. Sci. 9 (1974) 1715–1736, https://doi.org/10.1007/BF00540772.
[13] P. Singh, B. Venugopal, D. Nandini, Effect of electron beam irradiation on polymers, J. Mod. Mater. 5 (1) (2018) 24–33, https://doi.org/10.21467/jmm.5.1.24-33.
[14] U. Crossa Archiopoli, N. Mingolo, O.E. Martínez, Two-dimensional imaging of thermal diffusivity in metals by scanning photodeflection detection, J. Appl. Phys. 107 (2010), 023520, https://doi.org/10.1063/1.3289218.
[15] F. Zaldivar Escola, D. Kunik, O.E. Martínez, R. Kempf, N. Mingolo, Photothermal microscopy, Procedia Mater. Sci. 8 (2015) 665–673, https://doi.org/10.1016/j.mspro.2015.04.123.
[16] F. Zaldivar Escola, R. Kempf, N. Mingolo, O.E. Martínez, Characterization of sintered mixed oxides by photothermal microscopy, Int. J. Thermophys. 37 (20) (2016) 1–18, https://doi.org/10.1007/s10765-015-2027-8.
[17] F. Zaldivar Escola, O.E. Martínez, N. Mingolo, Microscopía fototérmica para el estudio de transformaciones de fase, Rev. Mat. 23 (2) (2018), https://doi.org/10.1590/s1517-707620180002.0369.
[18] D. Hansen, C.C. Ho, Thermal conductivity of high polymers, J. Polym. Sci. (3) (1965) 659–670, https://doi.org/10.1002/pol.1965.100030222.
[19] M. Luba, T. Pelt, R.G. Griskey, Correlating and predicting polymer thermal conductivities, J. Appl. Polym. Sci. 23 (1979) 55–58, https://doi.org/10.1002/app.1979.070230105.
[20] M.G. Kulkami, R.A. Mashelkar, Thermal conductivity of polymers: a new correlation, Polymer 22 (1981) 867–869, https://doi.org/10.1016/0032-3861(81)90258-5.
[21] X. Zhang, M. Fuji, Measurements of the thermal conductivity and thermal diffusivity of polymers, Polym. Eng. Sci. 43 (11) (2003) 1755–1764, https://doi.org/10.1002/pen.10148.
[22] W.N. dos Santos, Thermal properties of polymers by non-steady-state techniques, Polym. Test. 26 (2007) 556–566, https://doi.org/10.1016/j.polymertesting.2007.02.005.
[23] W.J. Parker, R.J. Jenkins, C.P. Butter, G.L. Abbot, A flash method of determining thermal diffusivity, heat capacity, and thermal conductivity, J. Appl. Phys. 32 (9) (1961) 1679–1684, https://doi.org/10.1063/1.1728417.
[24] W.N. dos Santos, P. Mummery, A. Wallwork, Thermal diffusivity of polymers by the laser flash technique, Polym. Test. 24 (5) (2005) 628–634, https://doi.org/10.1016/j.polymertesting.2005.03.007.
[25] H.S. Carslaw, J.C. Jaeger, Conduction of Heat in Solids, Oxford University Press., Oxford, 1959, https://doi.org/10.2307/3610347.
[26] W.E. Haupin, Hot wire method for rapid determination of thermal conductivity, Am. Ceram. Soc. Bull. 39 (3) (1960) 139–141.
[27] N. Mingolo, O.E. Martínez, Focus Shift photothermal method for thermal diffusivity mapping, J. Appl. Phys. 111 (12) (2012) 123526, https://doi.org/10.1063/1.4730636.
[28] E.A. Domené, F. Balzarotti, A.V. Bragas, O.E. Martínez, Photothermal measurement of absorption and scattering losses in thin films excited by surface plasmons, Opt. Lett. 34 (24) (2009) 3797–3799, https://doi.org/10.1364/OL.34.003797.
[29] N. Mingolo, O.E. Martínez, Thermal expansion recovery microscopy: practical design considerations, Rev. Sci. Instrum. 85 (2014), 014903, https://doi.org/10.1063/1.4863337.
[30] E. Perez, C. Bernal, C.J. Perez, Internal structure analysis of polypropylene/quartz composites related to their toughness, Polym. Compos. 37 (5) (2014) 1488–1496, https://doi.org/10.1002/pc.23318.
[31] Good Fellow Catalogue, Material information: (polypropilene), Retrieved from Argentina, http://www.goodfellow.com/E/Polypropylene.html, 2019. (Accessed 24 July 2019).
[32] Good Fellow Catalogue, Material information: (Quartz-Fused), Retrieved from Argentina, http://www.goodfellow.com/E/Quartz-Fused.html, 2019. (Accessed 24 July 2019).
[33] O.A. Sergeev, A.G. Shashkov, A.S. Umanskii, Thermophysical properties of quartz glass, J. Eng. Phys. 43 (6) (1982) 1375–1383, https://doi.org/10.1007/BF00824797.
[34] R. Yañez, J.D. Marconi, C. López, G.H. Rubiolo, S.N. Goyanes, Nuevo dispositivo para medición de difusividad térmica, Jor. SAM – CONAMET – AAS (2001) 795–802, 2001.
[35] S.M. Sarge, G.W.H. Höhne, W. Hemminger, Calorimetry, Wiley-VCH, 2014, https://doi.org/10.1002/9783527649365.